University of Bath

Monitoring individual wave characteristics in the inner surf with a 2-Dimensional laser scanner (LiDAR)

Kévin Martins[a], Chris E. Blenkinsopp[b], Jun Zang[c]

Research Unit for Water, Environment and Infrastructure Resilience (WEIR)
Department of Architecture and Civil Engineering
University of Bath, Claverton Down Road, Bath, BA2 7AY, UK
[a]k.martins@bath.ac.uk, [b]c.blenkinsopp@bath.ac.uk, [c]j.zang@bath.ac.uk

Abstract

This paper presents an investigation into the use of a 2-dimensional laser scanner (LiDAR) to obtain measurements of wave processes in the inner surf and swash zones of a microtidal beach (Rousty, Camargue, France). The bed is extracted at the wave-by-wave timescale using a variance threshold method on the time series. Individual wave properties were then retrieved from a local extrema analysis. Finally, individual and averaged wave celerities, are obtained using a crest-tracking method and cross-correlation technique respectively, and compared with common wave celerity predictors. Very good agreement was found between the individual wave properties and the wave spectrum analysis, showing the great potential of the scanner to be used in the surf and swash zone for studies of nearshore waves at the wave-by-wave timescale.

1. Introduction

1.1. LiDAR in coastal engineering

The use of remote sensing techniques in coastal engineering has become increasingly popular during the past 3 decades. These instruments can provide measurements at temporal and spatial scales that are not reached by common *in-situ* instruments. As an example, video imagery has been used for a wide range of applications: from bathymetric inversion (Stockdon and Holman, 2000) to alongshore swash motion variability (Guedes et *al.*, 2012).

Since remote sensors are non-intrusive instruments, they have the advantage of being easily and safely deployed on existing beachfront structures or specifically installed towers. Furthermore, instruments like the terrestrial LiDAR scanner (TLS) directly measure the wave profile and the wave properties (*e.g.* wave height and period) can subsequently be extracted. This represents an important advantage over other remote sensing techniques (*e.g.* video or radar) which are able to cover large domains but cannot directly obtain wave properties. Additionally, the ability of a single TLS to obtain data at multiple locations provides significant advantages over *in-situ* sensors like pressure transducers, which are commonly used in surf zone studies but provide only point measurements.

The first reported experiment using a TLS to study wave processes is that of Irish et *al.* (2006), who mounted a 4-rangefinder laser on a pier. A directional wave spectrum obtained with the scanner was compared to that from a submerged wave gauge, showing good agreement.

Recently, a few attempts were made to study the wave propagation or measure wave breaker heights. Harry et *al.* (2010) investigated the potential of a 3D TLS to capture the water surface of a surf zone. Despite capturing the wave profile successfully, the time spent by the scanner to scan on the three dimensions was a major drawback since it introduced an alongshore time shift on the wave crest propagation. Their conclusion was that a 2D TLS might be a better alternative. Park et *al.* (2011) also used a 3D TLS to measure breaker heights. They compared the scanner data with visual measurements against a vertical staff, and obtained a relatively good agreement over the 26 measured waves, with a Root Mean Square Error (RMSE) of 5 cm. Individual wave height and celerity measurement was also made possible by combining the use of video camera and a 3D TLS, fixed on an automated robot, in Wübbold et *al.* (2012). Interestingly, this technique enabled the measurement of several alongshore points of the wave crest, allowing a 2-dimensional description of the wave propagation.

Swash zone data have been obtained using fixed 2D TLS instruments by Blenkinsopp et *al.* (2010), Brodie et *al.* (2012) and Almeida et *al.* (2015), who demonstrated the ability of the instrument to measure swash hydro and morphodynamics with high accuracy. The approach of Wübbold et *al.* (2012) was also used by Vousdoukas et *al.* (2014) in laboratory conditions to measure wave-by-wave events in the swash zone. Overall, it was found that the precision of such instruments was lower than that of ultrasonic altimeters which had previously been used to make such swash measurements, however the ability to capture small scale features due to the high spatial resolution and small measurement footprint compared to other remote sensors make this instrument a powerful tool for coastal studies.

1.2. Known drawbacks of the 2D-LiDAR for wave processes studies

Previous studies (Blenkinsopp et *al.*, 2010; Evans, 2010) have shown that an aerated and turbulent water

surface is required for the laser to be sufficiently scattered to enable detection by the instrument. While in the laboratory, this can be achieved by adding particulates to increase the water turbidity (Allis *et al.*, 2011), this is not feasible in the field.

Fortunately, when the wave conditions are sufficiently energetic (wave breaking occurring), the surf and swash zones are very dynamic and are characterised by high levels of turbulence and aeration, which cause sufficient scattering for the consistent detection of the free surface elevation.

Environmental conditions (luminosity, air humidity, wind) also have an impact on the scanner measurements. While the influence of humidity or water drops, characterized by noise or spikes in data can be corrected, under high wind conditions the TLS can become too unstable for the data to be used. Indeed, while instrument accuracies are typically of the order of millimetres, the error induced by small oscillations of the instrument increases with distance from the instrument and can lead to measurement errors of the order of centimetres.

2. Experimental Setup

2.1. Site Location - Rousty

The experiment described in this paper was completed at Rousty beach, Camargue, which is located in the South of France on the Mediterranean Sea, from November 2014 until February 2015. The overall aim of the experiment was to study the coupling between the wave field, groundwater table dynamics and the beach morphodynamics. It was organised in two different phases: a 10-day short-term and high-frequency phase within a 3-month long period of low-frequency measurements.

The site presents morphodynamic characteristics typical of the beaches in the National park of Camargue (Sabatier, 2008; Sabatier *et al.*, 2009b). Despite the microtidal environment (tidal range ~0.4 m), this part of the coastline presents very dynamic beach/dune morphologies. This region is subject to seasonal storms accompanied by storm surges that flood the low-lying area of the Camargue beaches (Sabatier, 2008). This region is also exposed to very strong onshore wind episodes (mistral), which cause huge losses of sand due to aeolian transport (Sabatier *et al.*, 2009a).

The high-frequency part of the experiments took place from the 8th to the 18th of December 2014 (10 days). During this period, 15 buried pressure sensors were deployed on the berm located at approximately 60 m from the dune system in addition to a laser scanner fixed on top of a 4.8m-high tower erected at the shoreline, see Figure 1. Both sets of instruments were logged by a computer placed on a scaffold structure, 16 m landward of the scanner.

2.2. Instrumentation

In this section, only the scanner instrumentation will be described since this paper focusses on the capacity of a commercial 2D scanner for inner surf and swash zones studies. During the Rousty experiments, the TLS used was a commercial LMS511 Laser Measurement System manufactured by SICK. This ranging device uses the time of flight method: the distance between two objects is calculated using the time required for an eye-safe pulsed beam ($\lambda = 905$ nm) to be detected after reflection from the target. This instrument is similar to that used by

Figure 1: Photograph showing the experimental setup and their location on the upper part of Rousty beach. The TLS was fixed on the 4.8 meters-high tower standing on the left part of the picture while the scaffold is on the right. The buried sensors can be observed in between.

Blenkinsopp *et al.* (2010) in terms of its function and specification.

The TLS has a range of 65 m, a 190° field-of-view with an angular resolution of 0.1667°, and can be sampled at the sample rate of 25 Hz (SICK, 2015). With this sampling rate, each spatial measurement location is measured 25 times per second; the instrument thus providing a total of 28500 measured points per second. During the experiment, a 4.8m-high tower was erected around the shoreline position for mounting the scanner and from this position it was possible to obtain measurements across the whole beach profile and into the inner surf zone (approximately 30% of the surf zone was covered in the present dataset). A schematic of the high-frequency experimental setup can be observed in Figure 2.

For the experimental setup at Rousty and using an angular resolution of 0.1667°, the distance between measurement points varied from 0.014 m at the Nadir point (zero grazing angle) to 0.25 m at the most seaward valid measurement location (Figure 3). This spatial resolution allows the detection of the instantaneous shape of small wave features, something that most conventional, point-measurement instruments such as pressure transducers or wave gauges are unable to do. The systematic error and spot diameter provided by the manufacturer (SICK, 2015) are also shown in the same figure. The systematic error naturally increases with increasing spot diameter and evolves from ±0.025 m from 1 to 10 m from the scanner to ±0.035 m between 10 and 20 m.

As the grazing angle between the laser beam and the target decreases (α, Figure 2), the signal reflected by the water surface and returning to the scanner gets weaker. While bore fronts can still be captured due to a more normal-oriented surface relative to the instrument, a signal is not always returned from a more horizontal surface (*e.g.* wave troughs), resulting in increasing gaps in the dataset as we move offshore. As a result, a cross-shore position of -20 m relative to the TLS was set as the seaward extent of the dataset for the extraction of wave properties. If we consider a plane surface, the minimum incident angle allowing good quality data with this specific scanner model was found to be around 13.5°. It is noted however that, since wave crests could still be followed from further offshore, the bore celerities were calculated from -22
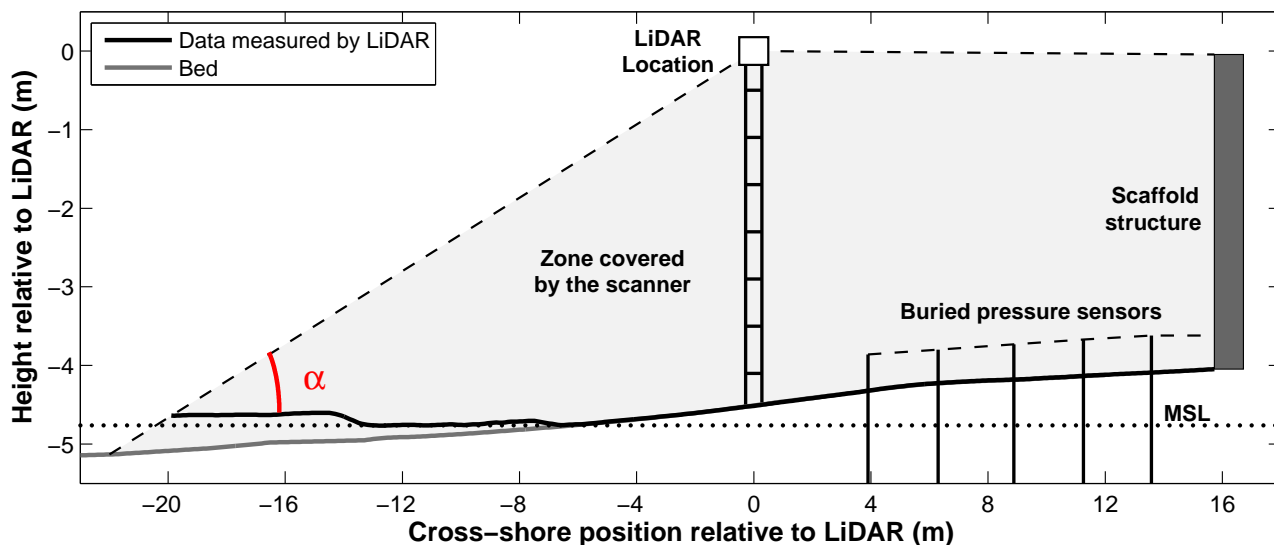
Figure 2: Schematic of the experimental setup at the Rousty experiments, for the 18 December 2014. The TLS, erected on top of a tower, covered a 35m-long zone from the scaffold structure where it was logged, to the point where the incident angle with the water surface (α) becomes too small for a sufficiently strong return signal. The cross-shore locations of the 15 buried pressure sensors are also shown (3 sensors were fixed to each buried pole, at different depth).

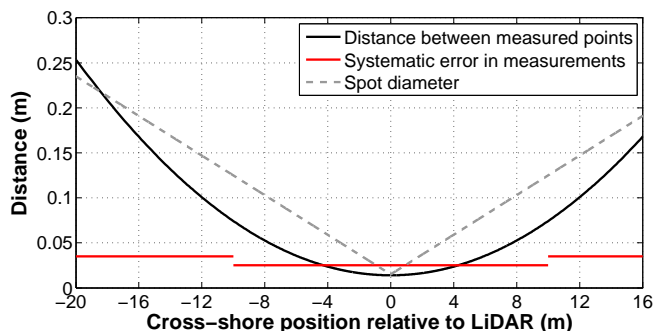m relative to the TLS, as discussed in Section 4.

Figure 3: Distance between the points measured by the TLS (black line), for this experimental setup described in this paper. This value evolves from 0.014 m at the Nadir to 0.25 m at the most seaward captured location. The systematic error and the spot diameter provided by the manufacturer are also plotted (red continuous and grey dashed lines respectively).

3. Methodology

3.1. Pre-processing

Before analysing the dataset to study wave characteristics in the inner surf and swash zones, pre-processing is required. As in Almeida et al. (2015), a beach survey carried out the same day as the dataset presented in this study (18 December 2014) was used to find the instrument orientation relative to the cross-shore profile. Data transformation from the scanner-centroid coordinate system to the cross-shore coordinate system is then possible from this analysis. This results in two arrays X and Z containing the cross-shore position and height relative to the scanner.

The dataset was de-spiked to reduce noise in the measurements and environmental effects such as splashes or people passing within the TLS field-of-view. De-spiking the time series was achieved using gradient thresholds between two consecutive points. Then to reduce random noise, the dataset was time-averaged using a moving-window method (0.2 s), and spatially interpolated onto a regular cross-shore grid ($\delta x = 0.1$ m).

3.2. Bed extraction

Since the instrument simply measures the distance to the closest target, no distinction on the medium is made, e.g. water or sand. Due to the scanner's location in the swash zone which is alternatively dry and submerged, an important step in the data processing is to separate the water signal from the bed. The methodology used in this study to extract the bed follows the work of Almeida et al. (2015).

Almeida et al. (2015) calculated the time series variance over 4-second windows at every point on the regular grid. This methodology relies on the fact that the time series variance when the target is the exposed bed is much smaller than that from a moving water surface. Therefore, by defining empirical thresholds at every cross-shore location, one can extract data corresponding to stationary, dry bed. By defining a water-depth criterion (0.015 m in this study) one can separate the original time series into separate 'bed' and 'wet' time series. This water-depth criterion ensures that the noise in the measurements (of the order $O(\text{mm})$) is not interpreted as 'wet' data.

By interpolating in time the extracted bed points, a beach profile can be obtained at each time step. This enables the monitoring of bed morphology at several hundred points and at the time scale of individual waves. An example of the result from this extraction is shown in Figure 4, where both accretionary and erosive swash events can be observed at $x = -10$ m.

3.3. Wave properties extraction

In order to obtain the individual wave characteristics at each point on the grid, a local maxima analysis was carried out on the surface elevation time series to detect the wave crests. This technique has been used in previous surf zone studies by Power et al. (2010) or Postacchini and Brocchini (2014) because it is insensitive to low-frequency motions, unlike most common methods such as zero-down crossing which define waves relative to intersection between the instantaneous free-surface elevation and mean sea level. When studying the surf zone, and especially the inner surf where low-frequency motions can be predom-
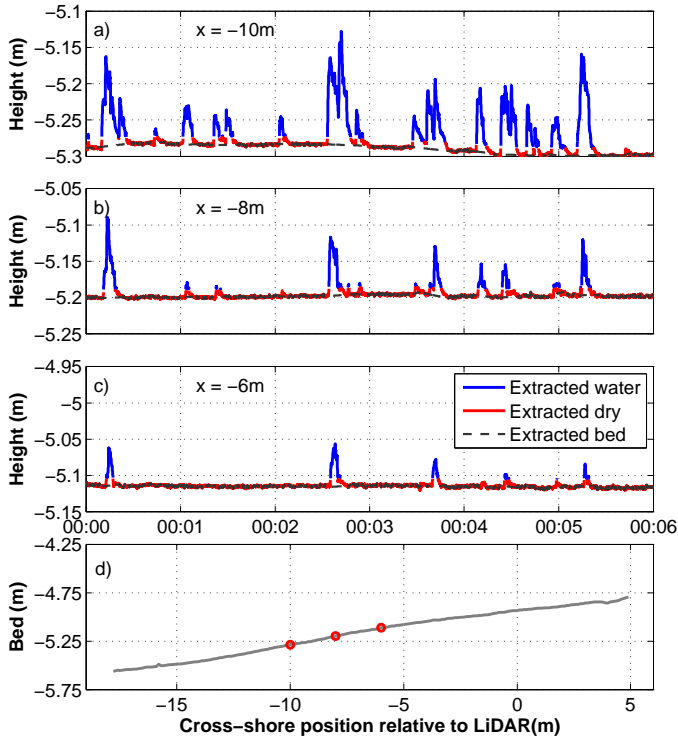
Figure 4: Example of bed extraction for the 14$^{\text{th}}$ of December. 3 cross-shore positions are shown in the panels (a), (b) and (c), and are represented by a red circle on the bed profile, in the panel (d). In blue is represented the 'wet' timeseries, in red the 'bed' one and in grey the time-interpolated bed. Interestingly, we can observe accretive and erosional patterns at the event time scale at the cross-shore position $x = -10$ m.

Figure 5: Example showing the wave extraction method in the inner surf zone. The wave-period-averaged water depth h_w contours are shown in (a), where red dots represent the detected wave crests. The orange lines are the waves selected in this time window for the celerity calculations. The panels (b), (c), (d) represent the water surface elevations at three cross-shore locations, with the chosen waves tracked across them. Extracted wave crests and troughs are represented by black circles and squares respectively.

inant, this aspect becomes critical since both the wave crest and trough can be under/above the defined mean water level. This is illustrated in Figure 5.

The wave troughs were defined as the minima reached between two crests and the wave period as the time elapsed between the passage of the troughs preceding and following a wave crest at the same location. A filter was applied to delete incorrect detections by limiting the time between 2 crests (2 s for this study). The wave height was defined as the elevation difference between the wave crest and trough elevations. Two other parameters were extracted, following the notation of Power et al. (2010): h_w the wave-period-averaged mean water depth (mean surface elevation between the two troughs immediately before and after a crest), and h_{tr} the trough depth. These are used for the analysis of individual wave celerities and the wave height to water depth ratio, γ.

3.4. Wave celerities

To calculate the wave celerities, two different approaches have been used. The first one was developed in the scope of this study and is based on a simple crest-tracking technique, allowing the estimation of individual wave celerities. The second uses a cross-correlation between two time series to calculate the averaged wave celerities over the time series length, following Tissier et al. (2011).

Individual wave celerities were calculated every 1 m between the cross-shore locations $x = -21$ and -10 m using a tracking algorithm. This algorithm is initiated by manually choosing waves at the cross-shore position $x = -22$ m and storing the corresponding time-index. At the next position ($x = -21$ m), the first detected crest
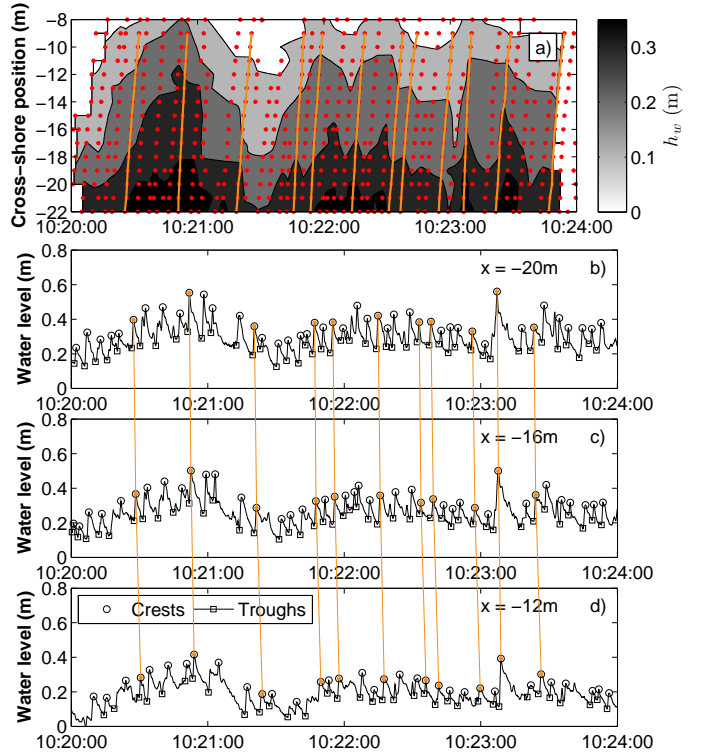
after this time index is assumed to be the same wave. The same methodology is used to track the wave until $x = -9$ m and every time-index is stored. The wave celerity at a cross-shore position x_i is then defined as the ratio of the distance between the two adjacent measurement points x_{i-1} and x_{i+1} (2 m) and the time elapsed between the passage of the wave crest at this two positions.

Due to the simplicity of the tracking algorithm and the difficulties caused by superposition of multiple waves within the inner surf, a careful visual inspection was carried out on all of the detected crests. Only waves not presenting obvious visual wave-wave interactions with other crests were selected. For the current study, this still enabled the detection of 275 waves and thus more than 3000 individual wave celerities. The process described above is illustrated for a 4-minute-period in Figure 5a, where the selected waves for this time window are shown in orange.

Averaged wave celerities were calculated following the method of Tissier et al. (2011). The cross-correlation was calculated between two 10-minute time series from two cross-shore locations (separated by 2 m). The maximum correlation found between the two time series is the averaged time delay between the surface elevation features. Physically, it represents an estimation of the averaged wave celerity over the time series.

Using these two different methods to estimate the wave celerity is interesting in several aspects. The TLS data opens up the possibility to detect wave celerity and geometry in shallow water right up to the shoreline without any mathematical transformation on the measure-

ments (*e.g.* Radon transform in Almar *et al.* (2013)). The present dataset corresponds to shallower water than investigated by Tissier *et al.* (2011), thus the relationship between wave properties and celerity can be studied closer to the shoreline. Furthermore, the estimation of individual celerities will provide more insight into the dispersion of these values.

4. Results

4.1. Bed Monitoring

Following the methodology presented in Section 3.1, the bed morphology has been monitored using the bed time series. By subtracting the initial beach face profile from the measured profile at each time step, erosion/accretion patterns over the measurement period can be observed. An example is presented in Figure 6 where the erosion/accretion patterns are shown every minute, after window-averaging the extracted bed (15-second window), for the period of the 13th to the 14th of December (30 continuous hours). This corresponded to the most energetic period of the 10-day experiments (energy peak around 13pm on the 13th of December).

Offshore wave conditions were measured by a buoy[1] located 40 km west of Rousty beach, moored in a water depth of 30 m. Measured significant wave height and peak and mean spectral periods are shown in Figure 6a and 6b respectively. Mean water levels were obtained by a tidal gauge located at Fos-sur-Mer port[2] (20 km east of Rousty). Interestingly, we can observe the influence of the tide even in this microtidal environment (high tides at 12:55pm on the 13th, 1:25am and 1:35pm on the 14th). In addition to the direct influence on the mean sea level, a significant reason for these oscillations is thought to be the weaker energy dissipation during high tides on this low-sloping barred beach (Guedes *et al.*, 2011). During the first part of this storm event (9am to 6pm on the 13th of December), the swash zone profile flattened and experienced the strongest erosion (~0.15 m) between $x = -10$ and -5 m. When the conditions became milder, there is evidence of berm building centred around $x = -10$ m at a rate of approximately 10 mm/hr. This berm remained present until the end of the experiment, with evolving steepness depending on the offshore conditions.

4.2. Validation of the extracted wave-by-wave properties

The methodology to extract wave properties based on the extrema analysis was compared to a classic spectral analysis (Figure 7). Significant wave height H_s was calculated by means of a Fast-Fourier Transform on a 15-minute time series, between cutoff frequencies of 0.05 Hz and 0.5 Hz. H_s was compared to the averaged extracted wave height of the 1/3 highest waves $H_{1/3}$ from the wave-by-wave analysis described in section 3.3, over the same period. The mean extracted individual wave period $T_{i,m}$ was compared to the mean wave period $T_{01} = m_0/m_1$, which is the inverse of the centroidal frequency, where m_n is the nth spectral moment is defined as:

$$m_n = \int_0^\infty f^n E(f) df \qquad (1)$$

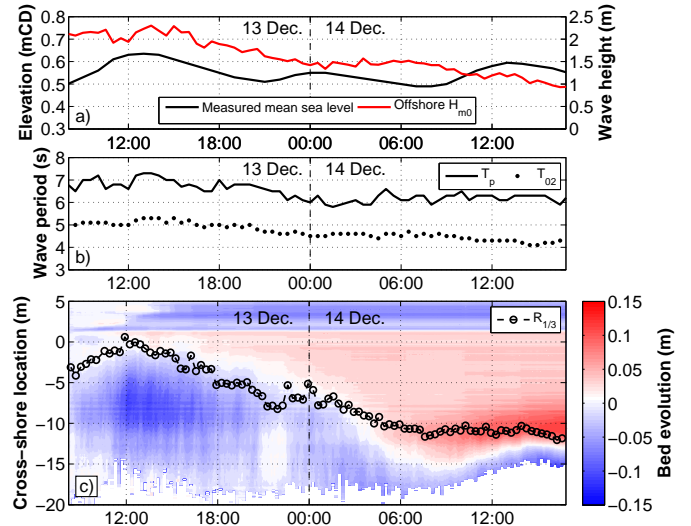with $E(f)$ the power density spectrum.

Figure 6: Bed extraction results: a) Measured mean water levels above Chart Datum at Fos-sur-Mer port and offshore significant wave height measured by a buoy close to Sete; b) Measured wave periods (T_p and T_{02}) by the same buoy; c) Beach morphological evolution for the 13th and 14th of December (30 continuous hours of measurement). Erosion and accretion patterns were calculated by subtracting the initial beach profile to that of the actual moment. Red color corresponds to accretion while blue corresponds to erosion. The significant runup limit $R_{1/3}$ is shown as a circled black line.
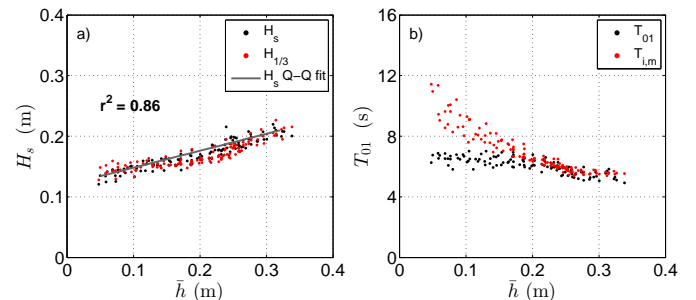

Figure 7: Comparison of a) significant wave heights and b) mean wave period calculated with two different methods: using the centroidal frequency inverse from spectral analysis (black dots) and averaged values over the same period of time, from an extrema analysis (red dots).

Plotted against the mean water depth over the same time period $\bar{h}$, H_s and $H_{1/3}$ show very good agreement at all water depths (Figure 7a), validating the extraction method based on the local extrema analysis. Both statistical ($H_{1/3}$) and spectral (H_s) significant wave height were found to show little scatter and to linearly decrease with averaged water depth ($r^2 = 0.86$). Though such depth-dependence is generally observed when saturated conditions are found in the inner surf (Sallenger and Holman, 1985), the relatively short dataset (2h30) and the consistent offshore conditions do not allow for such statement. Furthermore, waves were found to stop breaking and reform between the two beach bars, consistent with unsaturated conditions (Thornton and Guza, 1982).

In contrast to averaged values, measured individual wave heights showed considerably more scatter, see Figure 8a. This scatter is explained by two main factors: the influence of infra-gravity motions and the presence of high-frequency waves increasing or lowering the wave trough height. Naturally, it is also visible in the individual wave height to water depth ratio $\gamma_w = H/h_w$ (Figure 8b), which shows increasing values as waves approach

the shoreline, something previously observed by Sénéchal et al. (2004) and Power et al. (2010). In particular, the wide range of observed individual γ_w values show the inappropriateness of choosing constant values for this parameter in numerical models. Finally, the individual γ_w values, obtained closer to the shoreline than these two previous studies, seem to be in agreement with the line fit obtained with averaged γ_w values by Power et al. (2010).
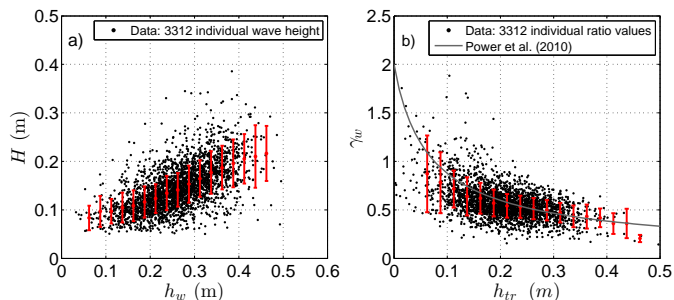

Figure 8: Individual wave properties: a) Wave height as a function of the wave-period-averaged water depth and b) wave height to water depth ratio as a function of the depth under the trough. Standard deviations are shown by the red bars and are calculated for 0.025m-wide bins. In b), the empirical fit equation obtained by Power et al. (2010) using averaged γ_w values is shown as the gray line.

The comparison between $T_{i,m}$ and T_{01} (Figure 7b) also shows interesting results. While for the deepest waters considered ($h \geq 0.2$ m), the mean extracted individual wave periods are consistent with T_{01}, as we get closer to the shoreline, the difference between the two values increases with decreasing water depth. This analysis gives some support to the idea of using the centroidal frequency to define a characteristic period in the inner surf, as suggested by Raubenheimer et al. (1996) and Sénéchal et al. (2004).

4.3. Influence of the characteristic period on the γ parametrization

To further compare the characteristic wave periods, the ratio between averaged significant wave height and water depths noted $\bar{\gamma}_s$ has been plotted against $\beta/\bar{k}\bar{h}$, which represents the fractional change in water depth over a wavelength. In this expression, β represents the bed slope, $\bar{k}$ the wave number calculated from the averaged estimated celerities and a characteristic period and $\bar{h}$ the averaged water depth over the same period.

Two different comparisons were made (using the same typology as in Section 4.2):
1. Comparison shown in Figure 9a using $H_{1/3}$ for $\bar{\gamma}_s$ and $T_{i,m}$ to derive $\bar{k}$.
2. Comparison shown in Figure 9b using H_s for $\bar{\gamma}_s$ and T_{01} to derive $\bar{k}$.

For both comparisons, a strong linear dependence was found between $\bar{\gamma}_s$ and $\beta/\bar{k}\bar{h}$. For deeper water and using two different frequency cutoffs, Raubenheimer et al. (1996) and Sénéchal et al. (2001) found similar linear relationship, but with different coefficients. For the present dataset and for both derived $\bar{\gamma}_s$, a good match is found with the linear fit obtained by Sénéchal et al. (2001) when $0 \geq \beta/\bar{k}\bar{h} \geq 0.5$. For greater values of $\beta/\bar{k}\bar{h}$, lower values compared to Sénéchal et al. (2001) are obtained when using the mean extracted wave period T_m, while that using T_{01} still match the linear fit. This limit value of $\beta/\bar{k}\bar{h}$ corresponds to the critical depth where T_{01} does

not match to $T_{i,m}$ any more (Figure 7b).

It is noted that the three compared datasets use different frequency cutoffs (0.05Hz $\leq f \leq$ 0.18Hz for Raubenheimer et al. (1996), 0.09Hz $\leq f \leq$ 0.3Hz for Sénéchal et al. (2001) and 0.05Hz $\leq f \leq$ 0.18Hz for the present study). Except for the influence of the much lower high frequency cutoff used by Raubenheimer et al. (1996), it is unclear why the present dataset shows higher values than in Raubenheimer et al. (1996) but matches that of Sénéchal et al. (2001). Finally, it has to be noted that the dataset presented in this study contains much shallower depths than that considered in the two previous studies. For instance, the highest value of $\beta/\bar{k}\bar{h}$ considered by the previous studies was 0.25 while it is approximately 1.75 in the current work.

4.4. Wave celerities

Individual wave celerities were compared to a range of previously developed predictors summarized in Table 1. In the different formulations, h, h_c, h_t are respectively the mean water depths, the crest height and the trough height. A more complete introduction to these predictors is given by Catálan and Haller (2008) who compared a wider range of celerity predictors against measurements obtained using video imagery from laboratory experiments.

Prior to this work, only a few studies have been published on the measurement of individual broken-wave celerities in the surf zone. Radon transform on video camera data have been used by Yoo et al. (2011) and Almar et al. (2014) to track wave crests, while Tissier et al. (2013) used a large array of wave gauges for this purpose. Additionally, Postacchini and Brocchini (2014) calculated individual broken-wave celerities by correcting the averaged celerities obtained by a cross-correlation method (Tissier et al., 2011) for each detected wave. While Tissier et al. (2011) found better agreement with Bonneton (2004) predictor using averaged celerities, individual celerities from Postacchini and Brocchini (2014) and this study were found to better match the solitary wave theory celerity, see Figure 10a.

In contrast to the study of Tissier et al. (2011) whose data was concentrated in the outer and mid-surf zone, the present study uses data from the inner surf to the swash zone. In particular, this enables one to look more closely at the boundary between the two zones in terms of wave celerities using the cross-correlation method. This is illustrated in Figure 10b, where the 10-minute averaged celerities are plotted against the corresponding averaged water-depth.

Between water depth of 0.2 and 0.4 m, the averaged celerities show good agreement with the modified shallow water wave predictor, though they are slightly underestimated. This is in agreement with the results found in Figure 10a. Indeed, the modified shallow water wave predictor corresponds to the solitary wave predictor with a constant wave height to water depth ratio of 0.78. Hence, despite a not-insignificant scatter when using the individual celerities (shown by Postacchini and Brocchini (2014), not shown in this study), the modified shallow water predictor provides good estimates of the averaged wave celerities seaward of $h \geq 0.2$ m, corresponding to $\gamma = 0.5$ in this study, see Figure 8b. Interestingly landward of this depth, averaged celerities remain quite constant, slightly decreasing, to finally present a much broader value range

Table 1: List of the different tested wave celerity predictors. For individual wave celerities, the mean water depth h, becomes the wave-period-averaged mean water depth h_w.

Predictor	Formulation of c
Linear theory (shallow water assumption)	$c = \sqrt{gh}$
Modified shallow water formulation (Schäffer et *al.*, 1993)	$c = 1.3\sqrt{gh}$
Solitary wave theory	$c = \sqrt{gh(1 + \dfrac{H}{h})}$
Bore model (Svendsen et *al.*, 1978)	$c = \sqrt{gh_c h_t \dfrac{(h_t + h_c)}{2h^2}}$
Shock model (Bonneton, 2004)	$c = -2\sqrt{gh} + 2\sqrt{gh_t} + \sqrt{gh_c \dfrac{(h_t + h_c)}{2h_t}}$

at the shoreline position ($1.3 \text{ m.s}^{-1} < c_b < 2.2 \text{ m.s}^{-1}$). This scatter of averaged values implies a wider range of individual celerities at the surf-swash boundary, which could be explained by the interaction between surf and swash processes.

5. Conclusion

In this study, a methodology for monitoring the beach morphology and individual wave characteristics using a shore-mounted 2-dimensional commercial laser scanner has been presented. The conclusions of this investigation can be summarized with the following points:

- The laser scanner can be used to measure time-varying water surface profiles in the inner surf and swash zones, enabling the study of wave propagation on a wave-by-wave as well as time-averaged basis.
- Individual wave properties (H, T) can be extracted using an extrema analysis on the measured time series. The extracted wave height was found to compare well with that from spectral analysis. It was also shown that for these conditions, the wave period derived from the centroidal frequency could be chosen as a characteristic wave period for water depths down to 0.2 m. Further investigation is needed on the reason why this changes at the swash/inner surf boundary.

- $\bar{\gamma}_s$ was found to be linearly dependent on $\beta/\bar{k}\bar{h}$. Furthermore, the present dataset seem to match well that of Sénéchal et *al.* (2001), for values of $\beta/\bar{k}\bar{h}$ lower than 0.5. For higher values, discrepancies are observed and are due to the differences observed between T_m and T_{01}.
- Individual wave celerities were estimated using a simple crest-tracking method. Comparisons with various predictors showed that the solitary wave theory gave the best agreement with the present dataset. However, in the shallow water depths investigated here, these values exhibit considerable variability.
- 10-minute averaged wave celerities were also calculated using a cross-correlation technique. These values agree well with the modified shallow-water predictor in depths greater than 0.2 m, becoming almost constant as the water depths decrease landwards. This critical depth also corresponds to that when T_m and T_{01} start to show discrepancies. Since the celerity is a function of the wave period, the two facts could be physically linked. This will be the subject of further investigation, since it could bring new insight into the conditions at the surf-swash boundary.
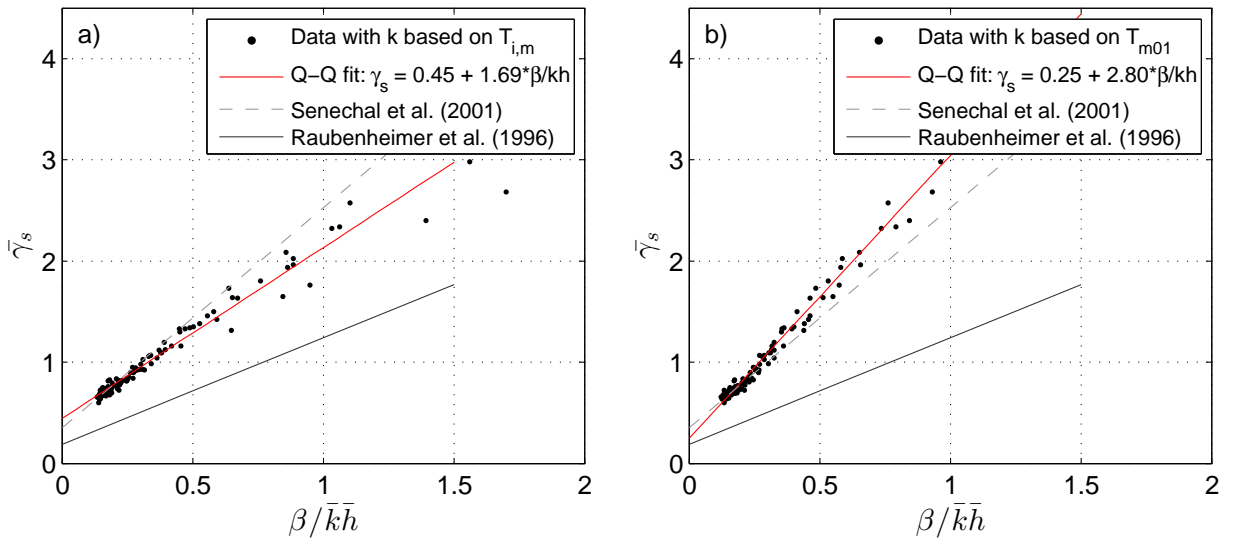

Figure 9: Averaged significant wave height to averaged water depth ratio plotted against $\beta/\bar{k}\bar{h}$: a) Ratio calculated with $\bar{k}$ based on the mean extracted individual wave period $T_{i,m}$; b) Ratio calculated with $\bar{k}$ based on the mean spectral wave period $T_{01} = m_0/m_1$, inverse of the centroidal frequency. The present dataset (black dots, and its Q-Q fit shown as red line) is compared to the fit obtained in two previous studies: dashed gray lines for Sénéchal et *al.* (2001) and gray continuous line for Raubenheimer et *al.* (1996).
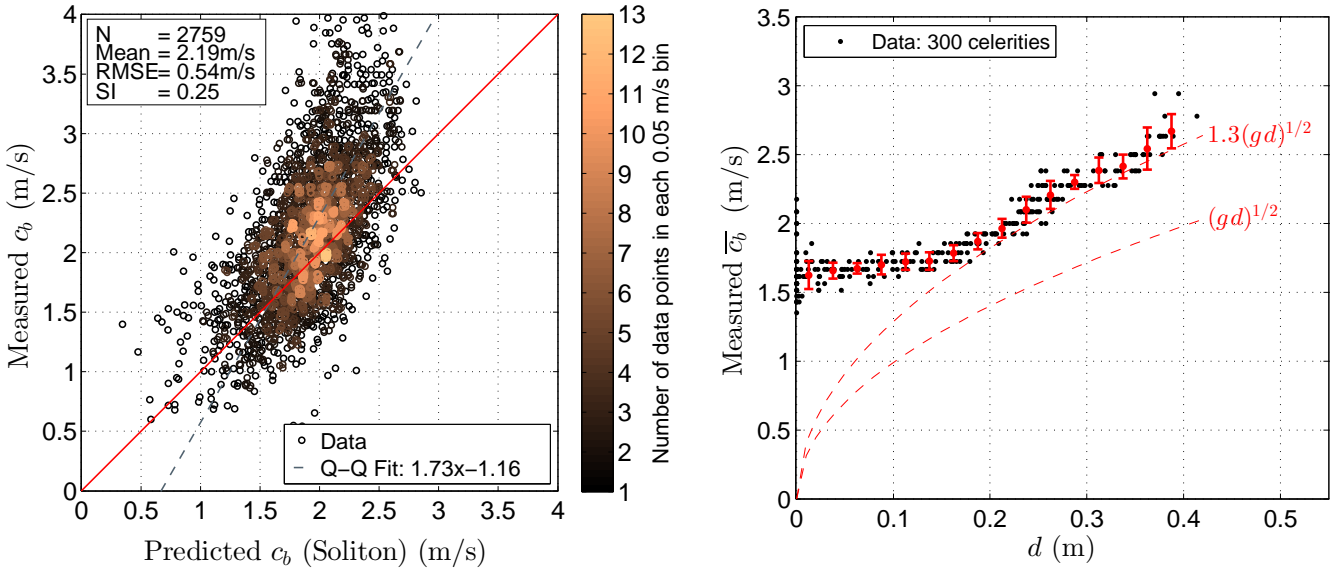
Figure 10: Scatter plot of measured wave celerities: a) individual wave celerities against the predictor from the solitary wave theory. Data circles are coloured by their concentration in every 0.05 m/s bins. The wave-period-averaged depth is used for the soliton celerity formulation, following Postacchini and Brocchini (2014). Correlation coefficient r = 0.65.; b) Averaged wave celerities obtained from the cross-correlation of two 10-minute time series, plotted against water depth. Their standard deviation is plotted as red bars, using 0.025m-wide bins. The modified and original linear wave theories in shallow water are represented in red dashed lines.

Appendix A: Statistical parameters

The different statistical parameters (Root-Mean Square Error, Scatter Index and a correlation coefficient noted r) used in this study are defined in this section. If we denote the two compared series as $X = \{x_1, \cdots, x_n\}$ and $Y = \{y_1, \cdots, y_n\}$, they are defined as follows:

$$\text{RMSE} = \sqrt{\frac{1}{n} \sum_{i=1}^{n} (x_i - y_i)^2} \tag{2}$$

$$\text{SI} = \frac{\sqrt{\frac{1}{n} \sum_{i=1}^{n} (x_i - y_i - \overline{(X-Y)})^2}}{\overline{X}} \tag{3}$$

$$\text{r} = \frac{\sum_{i=1}^{n} (x_i - \overline{X})(y_i - \overline{Y})}{\sqrt{(\sum_{i=1}^{n} (x_i - \overline{X})^2)(\sum_{i=1}^{n} (y_i - \overline{Y})^2)}} \tag{4}$$

References

Allis, M.J., Peirson, W.L., Banner, M.L., 2011. Application of lidar as a measurement tool for waves, in: The Twenty-first International Offshore and Polar Engineering Conference, 19-24 June, Maui, Hawaii, USA, pp. 373–379.

Almar, R., Bonneton, P., Michallet, H., Cienfuegos, R., Ruessink, B.G., Tissier, M., 2013. On the use of the radon transform in studying wave dynamics, in: 7th International Conference on Coastal Dynamics, Arcachon, France. pp. 73–82. URL: https://hal.archives-ouvertes.fr/hal-00909132.

Almar, R., Michallet, H., Cienfuegos, R., Bonneton, P., Tissier, M., Ruessink, G., 2014. On the use of the radon transform in studying nearshore wave dynamics. Coastal Engineering 92, 24 – 30. doi:10.1016/j.coastaleng.2014.06.008.

Almeida, L.P., Masselink, G., Russell, P.E., Davidson, M.A., 2015. Observations of gravel beach dynamics during high energy wave conditions using a laser scanner. Geomorphology 228, 15 – 27. doi:10.1016/j.geomorph.2014.08.019.

Blenkinsopp, C.E., Mole, M.A., Turner, I.L., Peirson, W.L., 2010. Measurements of the time-varying free-surface profile across the swash zone obtained using an industrial (lidar). Coastal Engineering 57, 1059–1065. doi:10.1016/j.coastaleng.2010.07.001.

Bonneton, P., 2004. Wave celerity in the inner surf zone. COASTAL ENGINEERING CONFERENCE 29, 392.

Brodie, K.L., Slocum, R.K., McNinch, J.E., 2012. New insights into the physical drivers of wave runup from a continuously operating terrestrial laser scanner, in: Oceans, 2012, pp. 1–8. doi:10.1109/OCEANS.2012.6404955.

Catálan, P.A., Haller, M.C., 2008. Remote sensing of breaking wave phase speeds with application to non-linear depth inversions. Coastal Engineering 55, 93 – 111. doi:10.1016/j.coastaleng.2007.09.010.

Evans, A.J., 2010. Laser scanning applied to hydraulic modeling, in: International Archives of Photogrammetry, Remote Sensing and Spatial Information Sciences, Commission V Symposium, Newcastle upon Tyne, UK.

Guedes, R.M., Bryan, K.R., Coco, G., 2012. Observations of alongshore variability of swash motions on an intermediate beach. Continental Shelf Research 48, 61 – 74. doi:10.1016/j.csr.2012.08.022.

Guedes, R.M.C., Bryan, K.R., Coco, G., Holman, R.A., 2011. The effects of tides on swash statistics on an intermediate beach. Journal of Geophysical Research: Oceans 116. doi:10.1029/2010JC006660.

Harry, M., Zhang, H., Lemckert, C., Colleter, G., 2010. 3d spatial definition of a water surface, in: The Ninth ISOPE Pacific/Asia Offshore Mechanics Symposium, 14-17 Novem-

ber, Busan, Korea.

Irish, J.L., Wozencraft, J.M., Cunningham, A.G., Giroud, C., 2006. Nonintrusive measurement of ocean waves: Lidar wave gauge. Journal of Atmospheric and Oceanic Technology 23, 1559–1572. doi:`10.1175/JTECH1936.1`.

Park, H.S., Sim, J.S., Yoo, J., Lee, D.Y., 2011. Breaking wave measurement using terrestrial lidar: validation with field experiment on the mallipo beach, in: *Proceedings 11th International Coastal Symposium*, Journal of Coastal Research, Special Issue, No. 64, Szczecin, Poland. pp. 1718–1721.

Postacchini, M., Brocchini, M., 2014. A wave-by-wave analysis for the evaluation of the breaking-wave celerity. Applied Ocean Research 46, 15 – 27. doi:`10.1016/j.apor.2014.01.005`.

Power, H.E., Hughes, M.G., Aagaard, T., Baldock, T.E., 2010. Nearshore wave height variation in unsaturated surf. Journal of Geophysical Research: Oceans 115. doi:`10.1029/2009JC005758`.

Raubenheimer, B., Guza, R., Elgar, S., 1996. Wave transformation across the inner surf zone. Journal of Geophysical Research: Oceans (1978–2012) 101, 25589–25597.

Sabatier, F., 2008. Modélisation de l'impact du changement climatique sur l'érosion des dunes. application à la camargue. La Houille Blanche , 40–49.

Sabatier, F., Anthony, E.J., Héquette, A., Suanez, S., Musereau, J., Ruz, M.H., Regnauld, H., 2009a. Morphodynamics of beach/dune systems: examples from the coast of france. Géomorphologie: relief, processus, environnement , 3–22.

Sabatier, F., Samat, O., Ullmann, A., Suanez, S., 2009b. Connecting large-scale coastal behaviour with coastal management of the rhÃťne delta. Geomorphology 107, 79 – 89. doi:`10.1016/j.geomorph.2006.09.026`. coastal vulnerability related to sea-level rise.

Sallenger, A.H., Holman, R.A., 1985. Wave energy saturation on a natural beach of variable slope. Journal of Geophysical Research: Oceans 90, 11939–11944. URL: `http://dx.doi.org/10.1029/JC090iC06p11939`, doi:`10.1029/JC090iC06p11939`.

Schäffer, H.A., Madsen, P.A., Deigaard, R., 1993. A boussinesq model for waves breaking in shallow water. Coastal Engineering 20, 185 – 202. doi:`10.1016/0378-3839(93)90001-O`.

Sénéchal, N., Dupuis, H., Bonneton, P., 2004. Preliminary hydrodynamic results of a field experiment on a barred beach, truc vert beach on october 2001. Ocean Dynamics 54, 408–414. doi:`10.1007/s10236-003-0052-9`.

Sénéchal, N., Dupuis, H., Bonneton, P., Howa, H., Pedreros, R., 2001. Observation of irregular wave transformation in the surf zone over a gently sloping sandy beach on the french atlantic coastline. Oceanologica Acta 24, 545 – 556. doi:`10.1016/S0399-1784(01)01171-9`.

SICK, 2015. Laser measurement sensors of the lms5xx product family - operating instructions URL: `https://www.sick.com/media/pdf/4/14/514/IM0037514.PDF`.

Stockdon, H.F., Holman, R.A., 2000. Estimation of wave phase speed and nearshore bathymetry from video imagery. Journal of Geophysical Research: Oceans 105, 22015–22033. URL: `http://dx.doi.org/10.1029/1999JC000124`, doi:`10.1029/1999JC000124`.

Svendsen, I.A., Madsen, P.A., Hansen, J.B., 1978. Wave characteristics in the surf zone. Coastal Engineering Proceedings 1.

Thornton, E.B., Guza, R., 1982. Energy saturation and phase speeds measured on a natural beach. Journal of Geophysical Research: Oceans (1978–2012) 87, 9499–9508.

Tissier, M., Almar, R., Bonneton, P., Michallet, H., Birrien, F., de Bakker, A., Ruessink, G., 2013. Individual wave celerity in the surf zone of a low-sloping laboratory beach, in: Proceeding of Coastal Dynamics 2013.

Tissier, M., Bonneton, P., Almar, R., Castelle, B., Bonneton,

N., Nahon, A., 2011. Field measurements and non-linear prediction of wave celerity in the surf zone. European Journal of Mechanics - B/Fluids 30, 635 – 641. doi:`10.1016/j.euromechflu.2010.11.003`. special Issue: Nearshore Hydrodynamics.

Vousdoukas, M.I., Kirupakaramoorthy, T., Oumeraci, H., de la Torre, M., WÃijbbold, F., Wagner, B., Schimmels, S., 2014. The role of combined laser scanning and video techniques in monitoring wave-by-wave swash zone processes. Coastal Engineering 83, 150 – 165. doi:`10.1016/j.coastaleng.2013.10.013`.

Wübbold, F., Vousdoukas, M., Hentschel, M., Wagner, B., 2012. Towards autonomous coastal monitoring using 3d laser range scanners and camera vision, in: 33rd International Conference on Coastal Engineering, Santander, Spain.

Yoo, J., Fritz, H.M., Haas, K.A., Work, P.A., Barnes, C.F., 2011. Depth inversion in the surf zone with inclusion of wave nonlinearity using video-derived celerity. Journal of Waterway, Port, Coastal, and Ocean Engineering 137, 95–106. doi:`10.1061/(ASCE)WW.1943-5460.0000068`.